International Journal of Computational and Experimental Science and ENgineering (IJCESEN)

Vol. 12-No.1 (2026) pp. 870-883
http://www.ijcesen.com

ISSN: 2149-9144

Research Article

Biogenic Synthesis and Characterization of Zinc Oxide and Titanium Dioxide Nanoparticles Mediated by Plant Extracts

Sabrina. Benmebarek[1*], Nadia Djouambi[2], Salima. Bacha[3], Imed Eddine Benmebarek[4], Bouzid Omar Boussaha[5], Aicha Beya Mammeria[6], Rabab Kadri[7]

[1]**Sabrina. Benmebarek,** Materials and Environmental Sciences Laboratory, Faculty of Science, Department of Material Science, University of Algiers Benyoucef Benkhedda, Algeria.
* **Corresponding Author Email:** s.benmebarek@univ-alger.dz – **ORCID:** 0009-0008-6944-2639

[2]**Nadia Djouambi,** Department of Material Science, University of Algiers Benyoucef Benkhedda, Algeria.
Email: n.djouambi@univ-alger.dz – **ORCID:** 0000-0002-1638-3822

[3]**Salima. Bacha,** Materials and Environmental Sciences Laboratory, Faculty of Science, Department of Material Science, University of Algiers Benyoucef Benkhedda, Algeria.
Email: s.bacha@univ-alger.dz **–ORCID:** 0009-0007-9461-7616

[4]**Imed Eddine Benmebarek,** *Department of Inorganic, Organic, and Biochemistry, Faculty of Chemical Sciences and Technologies, University of Castilla-La Mancha, Ciudad Real, 13005, Spain*
Email: imed.benmebarek@uclm.es – **ORCID:** 0009-0005-1961-6272

[5]**Bouzid Omar Boussaha,** Materials and Environmental Sciences Laboratory, Faculty of Science, Department of Material Science, University of Algiers Benyoucef Benkhedda, Algeria.
Email: b.boussaha@univ-alger.dz – **ORCID:** 0000-0002-4219-526X

[6]**Aicha Beya Mammeria,** Faculty of Science, Department of Natural and Life Sciences, University of Algiers Benyoucef Benkhedda, Algeria.
Email: ab.mammeria@univ-alger.dz – **ORCID:** 0000-0001-9979-3511

[7]**Rabab Kadri,** Faculty of Science, Department of Material Science, University of Algiers Benyoucef Benkhedda, Algeria.
Email: rabab.kadri3@gmail.com– **ORCID:** 0000-0001-9979-3577

Article Info:

DOI: 10.22399/ijcesen.4379
Received : 25 December 2025
Revised : 12 February 2026
Accepted : 15 February 2026

Keywords

Nanoparticles,
medicinal plant extract
antimicrobial activity
product development
environmental civilization

Abstract:

Nanotechnology is a multidisciplinary research field encompassing physics, chemistry, biology, and other disciplines, that focuses on the behavior of nanometric elements. It holds considerable importance in biomedical and dental applications, as nanoparticles are widely used in numerous applications due to their unique properties. The green synthesis of nanoparticles, particularly those based on plant extracts, has become an emerging area within nanotechnology and offers various benefits to humans. Metal oxide nanoparticles possess remarkable photocatalytic, magnetic, and antimicrobial properties thanks to their small size and large specific surface area. Zinc oxide and titanium dioxide nanoparticles generate reactive oxygen species, degrading pollutants and eliminating microorganisms. In this study, zinc oxide and titanium dioxide nanoparticles were synthesized using aqueous extracts of clove, olive leaves, lemon leaves, and mint, with zinc nitrate as a precursor and titanium dioxide chosen for its ability to catalyze chemical reactions and its effectiveness in removing environmental contaminants. Notably, herbal oral treatments offer potentially lower toxicity and antibacterial properties for treating oral infections. Various experimental techniques were employed for the preparation, characterization, and analysis of these nanoparticles, highlighting the environmentally friendly approach adopted in their synthesis. X-ray diffraction (XRD), FTIR spectroscopy, UV-visible spectroscopy and bioelectrical impedance analysis (BET) were used to characterize the optical, chemical, crystalline, textural, and elemental properties of the formed nanoparticles. The produced ZnONP and TiO2NP were tested for their

antimicrobial activity using a well diffusion technique against oral pathogens. The ZnONP and TiO2NP synthesized in green were initially confirmed using a UV-visible spectrophotometer. The analysis allowed for a comparison of the absorption bands of the two types of nanoparticles, eliminating interference from the solvent or reference substrate and providing an accurate absorption spectrum of the studied nanoparticles. Further analyses were performed on these nanoparticles, such as infrared (IR) spectroscopy, which allowed us to identify the functional groups involved in nanoparticle stabilization. X-ray diffraction (XRD) was used to determine the crystalline structure and crystallite size of the nanoparticles. The Brunauer-Emmett-Teller (BET) technique was used to measure the specific surface area of the nanoparticles, crucial data for catalytic and absorptive applications. Antibacterial activity was tested for zinc oxide (ZnO NPs) and titanium dioxide (TiO_2 NPs) nanoparticles synthesized from plant extracts using three bacterial strains.

1. Introduction

Oral health is a crucial pillar of overall well-being, influencing both quality of life and systemic health. Since ancient times, humans have used medicinal plants to treat various ailments, particularly in dentistry, where they are used to eliminate bacteria, reduce inflammation, soothe irritations, and relieve pain **[1]**. Formulations such as herbal mouthwashes have demonstrated promising effects in reducing oral biofilm, thanks to the richness of certain plants like clove, thyme, bay laurel, neem, and aloe vera, which are rich in bioactive compounds such as tannins, catechins, and sterols **[2]**. These compounds possess significant antimicrobial, anti-inflammatory, and antioxidant properties, contributing to the prevention and treatment of oral diseases. However, the therapeutic efficacy of these natural extracts can be limited by their low bioavailability and the variable stability of their active ingredients. It is in this context that nanotechnology appears as a revolutionary advance, particularly in the biomedical and analytical chemistry fields. It plays a crucial role in drug delivery, diagnostic techniques, antibacterial treatments, wound care, and the management of diseases such as cancer, heart disease, diabetes, and kidney disease. The incorporation of various nanoparticles synthesized from plants is an emerging method whose medicinal benefits are still unknown. The improvement of medical applications of nanobiotechnology has marked the beginning of a new era in nanomedicine by introducing the idea of controlling and treating human biological systems using nanomaterials **[3-4]**. Nanoparticles, typically zinc oxide (ZnO) and titanium dioxide (TiO_2), are distinguished by their excellent antimicrobial properties, biocompatibility, and ability to precisely target pathogens, while remaining safe for human tissues. The green synthesis method, using plant extracts as reducing and stabilizing agents, constitutes an ecological alternative to conventional chemical methods, thus reducing toxicity and environmental impact **[5]**.

Metal oxide nanoparticles possess remarkable properties such as photocatalytic, magnetic, and antimicrobial effects due to their small size and large specific surface area. Zinc oxide and titanium dioxide generate reactive oxygen species, degrading pollutants and eliminating microorganisms, while Fe_3O_4, with its superparamagnetism, has promising biomedical and environmental applications **[6]**. The optical properties of nanoparticles are also very interesting. Because their dimensions are smaller than the wavelengths of visible light (380–780 nm), they reduce the absorption and scattering of light, thus modifying the optical properties of certain materials. In the form of a thin layer, they appear transparent. Certain nanoparticles, such as metal oxides (ZnO, TiO_2) with diameters between 30 and 80 nm, are used as sunscreens due to their ability to absorb ultraviolet radiation while remaining transparent to the naked eye **[7]**. These properties are the basis for their numerous applications in dermo-cosmetics **[8]**. ZnO is a semiconductor with a wide band gap (~3.37 eV), which makes it effective for UV absorption. Under UV irradiation, it generates electron-hole pairs that react with water and oxygen to produce reactive oxygen species (ROS), capable of degrading various organic pollutants **[9]**. TiO_2, particularly in its anatase form, is widely used as a photocatalyst. Under UV irradiation, it generates ROS capable of decomposing organic compounds and inactivating microorganisms **[10]**. ZnO nanoparticles exert an antimicrobial effect by releasing Zn^{2+} ions and generating ROS, thereby disrupting bacterial cell membranes and leading to their death **[11]**. Through ROS production under UV irradiation, TiO_2 exhibits effective antimicrobial properties against various microorganisms, including antibiotic-resistant bacteria **[12]**.Clove, the dried flower bud of the clove tree (*Syzygium aromaticum*), belongs to the Myrtaceae family **[13]**. This tropical tree is rich in several bioactive compounds with specific therapeutic properties. Among the most important compounds are eugenol, acetyleugenol, and β-caryophyllene. These substances exhibit numerous activities, including

antibacterial, antifungal, acaricidal, antioxidant, and gastroprotective properties. They are responsible for the beneficial effects used in many medical treatments, such as the treatment of oral and dental infections, the reduction of pain and inflammation, cellular protection against free radicals, and protection against neurodegenerative diseases **[14]**.Olive leaves come from *Olea europaea*, a Mediterranean tree belonging to the *Oleaceae* family **[15]**. Modern research has highlighted several biological and pharmacological activities of olive leaf extracts, confirming their effectiveness in treating various pathologies. Their main activities include antioxidant effects, antimicrobial properties, anti-inflammatory effects, antiviral properties, and cancer prevention **[16]**.Lemon leaves belong to the *Rutaceae* family, which includes citrus fruits like the lemon tree (Citrus limon), and other plants such as kaffir lime and trifoliate orange (Poncirus trifoliata). The lemon tree is a fruit-bearing shrub with multiple uses, both culinary and medicinal **[17]**. It is rich in antioxidants and vitamin C, which can be used as ingredients in dietary supplements and medications. It contains a significant amount of bioactive compounds, such as monoterpenes and sesquiterpenes like limonene (D-limonene), sabinene, β-ocimene, carene, citronellal, citronellol, etc., and exhibits numerous promising activities, including antioxidant, antibacterial, and anticancer activity **[18]**.Mint is an aromatic herbaceous plant of the genus *Mentha*, belonging to the *Lamiaceae* family. It contains menthol, an organic compound naturally present in peppermint and other mint plants **[19]**. It also contains various secondary metabolites such as p-coumaric acid, furfural, several phenolic compounds, anthocyanins, phytosterols, organic acids, as well as methylheptenone and isopulegol. Mint exhibits several activities, including significant antimicrobial and antioxidant activity, anti-inflammatory, analgesic, and digestive properties, antispasmodic activity, and potential antitumor activity **[20]**.This study focuses on the green synthesis method for producing metal oxide nanoparticles (ZnONP and TiO2NP) which is cost-effective and environmentally friendly using extracts of clove, olive leaves, lemon leaves and mint due to their antimicrobial, anti-inflammatory and antioxidant qualities.

2- Materials & Methods

2.1- Materials

2.1.1- Plant Extract: Clove, olive leaves, lemon leaves, and mint were harvested, cleaned, and cut for the preparation of the extracts.

2.1.2- UV-Visible Absorption Spectroscopy: The optical properties of the synthesized ZnO and TiO2NP nanoparticles were studied using a Perkin Elmer UV-Visible spectrophotometer (model Lambda 25). The analysis was performed in a wavelength range from 200 nm to 350 nm, allowing for the examination of the characteristic electronic transitions of the nanoparticles. This spectrophotometer is equipped with a dual-beam system.

2.1.3- Infrared Spectroscopy (IR): The infrared spectroscopy analysis was performed using the Perkin Elmer Spectrum Two spectrophotometer. The nanoparticle samples were mixed with paraffin and then deposited between two NaCl plates. The spectrum was recorded in a wavelength range of 400 to 4000 cm^{-1}.

2.1.4- X-ray Diffraction (XRD): The crystal structure of the ZnO and TiO_2 nanoparticles was analyzed using a Malvern PANalytical Empyrean diffractometer, renowned for its high performance in the analysis of powders, thin films, nanomaterials, and bulk solids. The samples, in the form of a homogeneous fine powder, were deposited on a special flat sample holder and then subjected to analysis. The system uses Cu Kα radiation (λ = 1.5406 Å), and data were collected over an angular range of 2θ from 10° to 80°. The obtained spectra were compared to standard maps in the JCPDS database for crystalline phase identification. The average crystallite size was calculated using the Scherrer equation, based on the most intense peaks.

2.1.5- Brunauer-Emmett-Teller (BET): The specific surface area of the nanoparticles was determined using the BET method. Before analysis, the samples underwent degassing under vacuum (or nitrogen) for 6 hours at specific temperatures: 180 °C for ZnO, 250 °C for TiO_2. This step is essential to remove moisture and adsorbed gases, thus ensuring the accuracy of the surface area measurements.

2.1.6- Antibacterial effect of nanoparticles: three bacterial strains were used for the antibacterial effect test: *Staphylococcus aureus, Escherichia coli* and *Pseudomonas aeruginosa*, isolated from contaminated samples.

2.2- Methods

2.2.1- Preparation of plant extracts: Mint and lemon leaves were harvested and thoroughly washed with distilled water to remove impurities and contaminants. 50 g of each fresh leaf was taken and cut into small pieces using sterile scissors, then

transferred to a clean beaker containing 400 ml of distilled water. The beaker was then placed on a hot plate at a temperature between 60°C and 70°C for 30 to 45 minutes, with moderate stirring. After extraction, the mixture was cooled and filtered using Whatman No. 1 filter paper (Whatman Plc, Maidstone, UK). The filtrate represents the aqueous extract used for the synthesis of nanoparticles. The same procedure was followed with clove and olive leaves **[21-22]**.

2.2.2- Preparation of ZnONP: 200 ml of the aqueous plant extract was heated in a water bath to a temperature of 55-60°C. Then, 20 g of zinc nitrate, dissolved in 100 ml of distilled water, was added to the plant extract. The resulting solution was heated for 45 minutes at 55-60°C with continuous stirring. The ZnO nanoparticle (NP) solution was then dried in a heating mantle. Once the solution was completely dried, the residue contained ZnO nanoparticles, unreacted zinc nitrate, and phytochemicals. The dry residue was washed with distilled water to remove the unreacted zinc nitrate. The solid was then washed with ethanol to remove the unreacted phytochemicals. Finally, the remaining solid was dried at room temperature. To obtain pure ZnO nanoparticles, a heat treatment (calcination) was carried out at 500°C for 4 hours. At the end of this treatment, a fine, odorless white powder was obtained, thus constituting the purified ZnO nanoparticles **[23-24]**.

2.2.3- Preparation of TiO_2NPs: 8 grams of titanium dioxide (TiO_2) were dissolved in 400 ml of distilled water and then heated on a hot plate to a temperature between 60°C and 80°C, with continuous stirring to ensure homogeneity. Once the temperature was reached, a previously prepared plant extract solution was slowly added to the TiO_2 mixture, while continuing to stir and maintaining the temperature between 70°C and 80°C for 3 hours. During this time, a color change was observed, from white to light brown with a yellowish tint, indicating the formation of nanoparticles. After this time, stirring was stopped, and a white precipitate formed at the bottom of the container, representing the nanoparticles. The precipitate was separated by filtration and then dried at 100°C until the solution had completely evaporated, leaving the nanoparticles dry. Finally, the nanoparticles were subjected to calcination in a muffle furnace at 550°C to ensure their crystallization and obtain pure TiO_2 nanoparticles **[25]**.

2.2.4- Characterization of nanoparticles: In this work, various characterization techniques were used to analyze the physicochemical, structural, and morphological properties of zinc oxide (ZnO) and titanium dioxide (TiO_2) nanoparticles synthesized via green processes. These techniques allow for a better understanding of the essential characteristics of the nanoparticles, such as their size, crystalline structure, specific surface area, elemental composition, and the functional groups present.

2.2.5- Antibacterial effect of nanoparticles: The antibacterial activity of ZnOnps and TiO_2nps nanoparticles, synthesized from plant extracts (clove, olive leaves, lemon leaves, and mint), was evaluated using the disk diffusion method. This method allowed us to study the effectiveness of the nanoparticles against three representative bacterial strains: Staphylococcus aureus, Escherichia coli, and Pseudomonas aeruginosa, isolated from contaminated samples. Mueller-Hinton (MH) culture medium was prepared according to the manufacturer's instructions and then poured into sterile Petri dishes before solidification. Each bacterial strain was cultured on the MH medium and then uniformly inoculated using a sterile swab to obtain a homogeneous growth surface. Sterile discs were then placed on the surface of the medium and impregnated with different nanoparticle suspensions: TiO_2 (lemon leaf/mint), TiO_2 (olive leaf/clove), ZnO (olive leaf/clove), and ZnO (lemon leaf/mint).The plates were incubated at 37°C for 24 hours. At the end of this period, antibacterial activity was assessed by measuring the diameters of the inhibition zones (clear areas formed around the discs). These zones reflect the ability of the nanoparticles to inhibit bacterial growth, thus allowing comparison of their efficacy depending on the nature of the nanomaterial and the plant extract used for synthesis **[26]**.

3- Results and discussion

3.1- Results

During the synthesis of the nanoparticles, and after heating combined with stirring for 45 min for ZnOnps and 3 h for TiO2nps, the solution becomes cloudy (**Fig. 1-A and B-1**). After a settling period, a solid deposit forms at the bottom of the beaker.

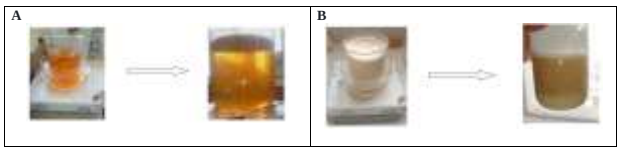

Figure 1: *Green synthesis of ZnOnp* ***(A)*** *and TiO2np* ***(B)*** *nanoparticles*

This phenomenon suggests a colloidal instability of the nanoparticles in the reaction medium leading to

their progressive aggregation and precipitation over time.

3.1.1- UV-Vis Characterization:

Plant extracts act not only as reducing agents but also as stabilizing agents. Zinc and titanium ions are reduced in zinc nitrate and titanium dioxide solutions, respectively, by secondary plant metabolites. This phenomenon was studied by UV-Vis spectroscopy between 200 and 400 nm. This technique highlights the characteristic electronic transitions of these materials, particularly the absorption bands associated with interband transitions. ZnO nanoparticles generally exhibit a marked absorption band in the 380–400 nm region, while TiO_2 nanoparticles absorb in a slightly narrower range, around 330–370 nm, depending on their size and crystal structure **[27]**.

a- UV-Vis Spectra of ZnO Nanoparticles: The spectrum in figure **2-A**, representing ZnOnp nanoparticles, shows a marked maximum absorbance between 380–400 nm, confirming better absorption in the near-UV region and the formation of ZnO synthesized with clove/olive leaves at the nanoscale. The spectrum (**Fig. 2-B**) shows a lower absorbance between 250–380 nm for ZnOnp synthesized with lemon/mint leaves, which may reflect a difference in particle structure or size **[28]**. The spectra exhibit a strong peak around 360–400 nm, characteristic of the band gaps of ZnOnp.

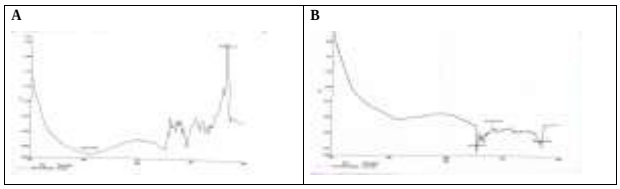

Figure 2: *UV-Visible spectrum of ZnOnp clove/olive leaves* ***(A)*** *and mint/lemon leaves* ***(B)***

The shift towards longer wavelengths (red band) in ZnOnp (clove/olive leaves) likely indicates larger particles or improved crystallinity. ZnOnp (lemon leaves/mint) shows a shift towards blue, indicating smaller particle sizes or a possible modification of the functional groups associated with the plant extracts.

b- UV-Vis spectrum of TiO_2 nanoparticles: TiO_2 nanoparticles exhibit a maximum absorbance at 356.94 nm (0.05 Å) and two minimum absorbance points at 327.17 nm (0.02 Å) and 384.11 nm (0.02 Å) for TiO_2np mint/lemon leaf (**Fig. 3-B**). A maximum absorbance at 368 nm (0.09 Å) and two minimum absorbance points at 327.16 nm (0.05 Å) and 383.96 nm (0.05 Å) for TiO_2np clove/olive leaf (**Fig. 3-A**). The profile is typical of a band gap transition of TiO_2 nanoparticles, particularly of the anatase phase **[29]**.

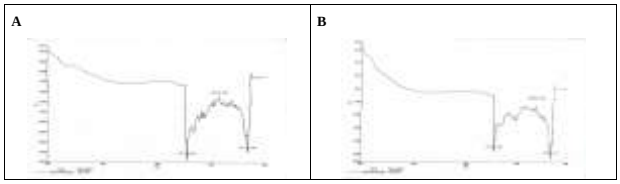

Figure 3: *UV-Visible spectrum of TiO_2np clove/leaves* ***(A)*** *and mint/lemon leaves* ***(B)***

3.1.2- IR Characterization:

In this work, infrared spectroscopy (FTIR) was used to confirm the formation of zinc oxide (ZnO) and titanium dioxide (TiO_2) nanoparticles synthesized using green chemistry by identifying the characteristic vibrations of chemical bonds, particularly Zn-O and Ti-O. Peaks appear in the 480–590 cm^{-1} and 680–780 cm^{-1} regions for ZnO and TiO_2, respectively, confirming the presence of these bonds. The spectra were obtained using the paraffin method, requiring particular attention to the characteristic bands of the paraffin **[30]**. A more in-depth characterization of the different bands formed initially requires clarification of the bands of ZnO (**Fig. 4-A**) and of the paraffin added to the samples (**Fig. 4-B**).

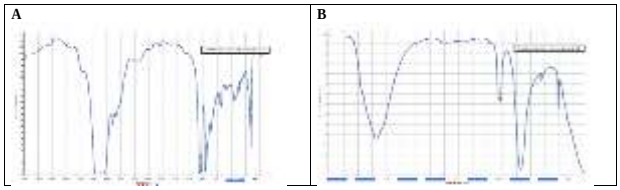

Figure 4: *Infrared spectrum of paraffin* ***(A)*** *and zinc nitrate $Zn(NO_3)$* ***(B)***

The paraffin spectrum (**Fig. 4-A**) shows peaks at positions 2916 and 2849 cm^{-1}, corresponding to the stretching vibrations of $–CH_2$, and peaks at positions 1462 and 1375 cm^{-1}, corresponding to the bending vibrations of CH_3 and CH_2. These peaks are interferences that must be eliminated when analyzing samples containing nanoparticles. Zinc nitrate (**Fig. 4-B**) is characterized by positions 1385 cm^{-1} and 825 cm^{-1}, corresponding to the vibrations of asymmetric NO_3^- and symmetric NO_3^-, respectively. The disappearance of these peaks in the ZnO samples confirms the complete conversion of Zn^{2+} ions to ZnO.

a-IR spectra of ZnO nanoparticles: The analysis of ZnOnp nanoparticles synthesized by the same method reflects the spectra below, (**Fig. 5-A and 5-B**), with the following extracts: olive leaves/clove, lemon leaves/mint.

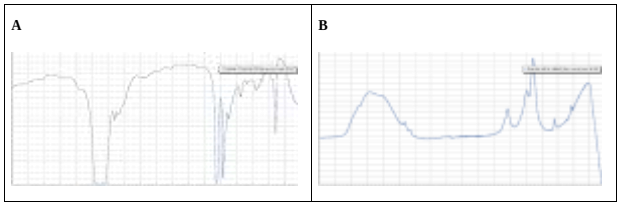

Figure 5: *Infrared spectrum of ZnOnp* ***(A)*** *olive leaves/clove and lemon leaves/mint* ***(B)***

The different vibrations of the ZnOnp nanoparticles are shown in **Table 1**, **[31]**:

Table 1: *Different vibrations of ZnOnp nanoparticles*

Extract from medicinal plants	Position (cm^{-1})	Attribution	Interpretation
Olive leaves / cloves	3432	ν(OH)	Tannins, phenols
	1620	C=O, C=C	Aromatic compounds
	1400–1350	CH_3, C–N	Traces of protein
	1080	C–O–C	Glycosides
	520–490	Zn–O	Confirmed ZnO formation
Lemon leaves / mint	3415	ν(OH)	Hydroxyl compounds
	1625	C=O, C=C	Polyphenols
	1385	CH_3, C–N	Plant-based proteins
	1095–1040	C–O	Ethers or alcohols
	515–480	Zn–O	ZnO characteristic band

b- IR spectra of TiO_2 nanoparticles: The spectra below accurately indicate the infrared absorptions of the different functional groups, specifying the bond involved. The vibration type, wavenumber range, and intensity of the synthesized TiO_2NPs are shown in green, with the following extracts: olive/clove leaves and lemon/mint leaves (**Fig. 6-A and 6-B**), **[32]**.

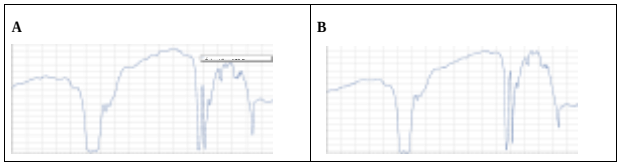

Figure 6: *Infrared spectrum of TiO_2np from olive/clove leaves* ***(A)*** *and lemon/mint leaves* ***(B)***

The different vibrations of TiO_2np nanoparticles (**Table 2**):

Table 2: *Different vibrations of TiO_2np nanoparticles*

Extract from medicinal plants	Position (cm^{-1})	Attribution	Interpretation
Olive leaves / cloves	3423	ν(OH)	Phenols (oleuropein, eugenol)
	1618	C=C aromatique	Phenolic compounds
	1430–1380	CH_3, C–N	Protein traces
	1118–1035	C–O, C–OH	Glycosides, tannins
	780–600	Ti–O	Confirmed formation of TiO_2
Lemon leaves / mint	~3410	ν(OH)	Polyphenols, flavonoids
	1632	ν(C=O) ou C=C	Aromatics, carbonyl compounds
	1392	δ(CH_3), C–N	Alkaloids, proteins
	1070	C–O	Secondary alcohols
	683–780	Ti–O–Ti	Formation of TiO_2

3.1.3- X-ray diffraction analysis of the synthesized nanoparticles in green

X-ray diffraction analysis was performed to determine the crystalline nature and phases present in the synthesized TiO_2 and ZnO nanoparticles. This technique allows for the precise identification of crystalline structures based on characteristic peaks appearing at specific angles. It is essential for confirming the formation of crystalline phases. Furthermore, XRD analysis provides information on the crystallinity and average size of the crystallites, crucial parameters for the material's functional performance.

a- Diffractogram of ZnO: The combined use of clove/olive leaf extracts is rich in bioactive compounds such as eugenol, flavonoids, tannins, and phenols, which promote the nucleation and controlled growth of nanoparticles while avoiding toxic chemicals (**Fig. 7-A**). The use of mint/lemon leaf extracts allows them to act as natural reducing and stabilizing agents. These extracts are rich in polyphenols, flavonoids, carboxylic acids, and tannins, antioxidant compounds that promote the controlled formation of ZnO nanoparticles, while avoiding the use of toxic chemicals (**Fig. 7-B**). This green approach offers an ecological and sustainable alternative to conventional nanoparticle synthesis.

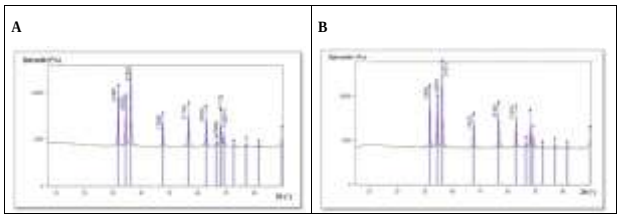

Figure 7: *ZnOnp diffractogram of clove /olive leaves* ***(A)*** *and mint /lemon leaves* ***(B)***

According to Figure **7-A**, the intense peak observed at $2\theta \approx 36.3°$ corresponds to the (101) crystal plane, characteristic of the hexagonal wurtzite phase of ZnO. Other notable peaks appear at approximately 31.8° (100), 34.5° (002), 47.5° (102), 56.6° (110), and 62.8° (103), confirming the good crystallinity and purity of the ZnO phase. The absence of spurious peaks or signals associated with other oxides or impurities suggests a specific and selective synthesis of ZnO, without the formation of byproducts.The diffractogram obtained for the ZnO nanoparticles shows intense and well-defined peaks, indicating good crystallinity of the material. Comparison with the reference data sheet JCPDS 98-016-5002 (corresponding to the wurtzite-type hexagonal phase of ZnO, also called zincite) confirms this identification **[33]**. The correspondence of the experimental peaks with the wurtzite phase of ZnO shown in **Table 3**:

Table 3: *X-ray diffraction parameters for the (hkl) planes of clove/olive leaf ZnO*

N°	Plan (hkl)	2θ (°)	d (Å)	Intensity (%)
1	(100)	31.78	2.8137	56.2
2	(002)	34.42	2.6035	43.4
3	(101)	36.26	2.4754	100.0
4	(102)	47.54	1.9110	24.0
5	(110)	56.61	1.6245	34.9
6	(103)	62.86	1.4772	30.8
7	(200)	66.39	1.4069	4.9
8	(112)	67.96	1.3782	27.5
9	(201)	69.10	1.3582	12.9

Crystalline structure and purity: The presence of sharp, well-resolved peaks indicates good crystallinity of the synthesized nanoparticles. The absence of peaks associated with other phases, such as $Zn(OH)_2$ or metallic impurities, confirms that the sample is composed exclusively of the pure ZnO phase (zincite). Compliance with JCPDS 98-016-5002 validates the hexagonal close-packed (wurtzite) structure, which is the thermodynamically stable phase of ZnO at room temperature. The crystallite size according to the Scherrer equation is D = 335 Å.According to Figure **7-B**, the intense main peak at 2θ ≈ 36.2° is typical of the (101) crystal plane, characteristic of the hexagonal wurtzite phase of ZnO. Other secondary peaks appear at approximately 31.8° (100), 34.4° (002), 47.5° (102), 56.6° (110), and 62.8° (103), also confirming this structure. No peaks associated with other phases such as $Zn(OH)_2$ or metallic impurities are visible, suggesting that the material is predominantly, if not exclusively, pure ZnO.The diffractogram obtained for the ZnO nanoparticles reveals several intense and well-defined peaks, characteristic of a crystalline material. Analysis of the angular positions of the peaks (2θ) shows a good correspondence with the data in JCPDS 98-016-5002, confirming that the material obtained is indeed ZnO in the hexagonal wurtzite phase **[33]**. Correspondence of the experimental peaks with the wurtzite phase of ZnO:

Table 4: *X-ray Diffraction Parameters for (hkl) Planes of Mint/Lemon Leaf ZnO*

N°	Plan (hkl)	2θ (°)	d (Å)	Intensity (%)
1	(100)	31.78	2.8137	56.2
2	(002)	34.42	2.6035	43.4
3	(101)	36.26	2.4754	100.0
4	(102)	47.54	1.9110	24.0
5	(110)	56.61	1.6245	34.9
6	(103)	62.86	1.4772	30.8

Crystalline structure and purity: The presence of sharp peaks without background noise indicates good crystallinity of the nanoparticles. The absence of additional or shifted peaks confirms the purity of the ZnO phase without the formation of impurities or secondary phases. The diffractogram profile also suggests a nanometric size of the crystallites, typical of green syntheses. The crystallite size according to the Scherrer equation is D = 335 Å.

b- Diffractogram of Ti2Onp: The use of clove/olive leaf extracts allowed them to act as natural reducing and stabilizing agents. These extracts contain phenolic compounds, tannins, and other antioxidants that facilitate the controlled formation of nanoparticles, while avoiding toxic chemicals (**Fig. 8-A**). The use of natural mint/lemon extracts influences the morphology, particle size, and crystallinity of TiO_2 (**Fig. 8-B**).

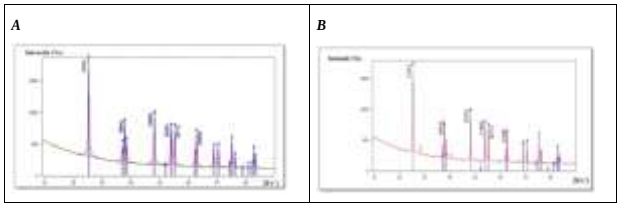

Figure 8: *Diffractogram of TiO2np from cloves and olive leaves* ***(A)*** *and mint/lemon leaves* ***(B)***

According to Figure **8-A**, the intense main peak at 2θ ≈ 25.3° is typical of the (101) crystal plane of the anatase phase. Other secondary peaks, at approximately 38.6° (112), 48.0° (200), 53.9° (105), and 62.7° (204), also confirm this structure. No peaks associated with the rutile (2θ ≈ 27.4°) or brookite phases are visible, suggesting that the material is predominantly, if not exclusively, in the anatase phase.The diffractogram obtained for the TiO_2 nanoparticles shows intense and well-defined peaks, characteristic of a crystalline material, belonging to the anatase phase. Comparison with the reference sheet JCPDS 98-017-2914 confirms this identification **[34]**. The correspondence of the experimental peaks with the anatase phase is shown in the table 5.

Table 5: *X-ray Diffraction Parameters for the (hkl) planes of clove/leaf TiO_2*

N°	Plan (hkl)	2θ (°)	d (Å)	Intensity (%)
1	(101)	25.31	3.517	100.0
2	(004)	37.80	2.378	20.1
3	(200)	48.04	1.893	27.3
4	(105)	53.90	1.700	17.3
5	(211)	55.06	1.667	17.2
6	(204)	62.69	1.481	13.3

The indexed plane (011) in the results is equivalent to plane (101) in the JCPDS nomenclature and represents the main peak of the anatase phase.

Crystal structure and purity: The presence of sharp peaks without background noise indicates good crystallinity of the material. The absence of peaks associated with the rutile (2θ ≈ 27.4°) or brookite phases proves that the sample is composed exclusively of the anatase phase. The crystallite size according to the Scherrer equation is D = 325.4 Å.

According to Figure **8-B**, the major peaks observed (25.32° (2θ)) in the XRD spectrum correspond to the characteristic crystal planes of the anatase phase of TiO_2, which is the most reactive and commonly used phase for photocatalytic applications. The absence or very low intensity of peaks corresponding to the rutile or brookite phases suggests that the synthesis favors the formation of the nearly pure anatase phase.The resulting diffractogram shows a series of peaks corresponding to well-defined crystal planes, characteristic of the anatase phase of titanium dioxide (TiO_2). To confirm this identification, the angular positions (2θ) and interplanar spacings (d) were compared to the data in JCPDS 98-008-2084, the reference for the anatase phase **[34]**. The correspondence of the experimental peaks with the anatase phase is shown in the table below:

Table 6: *X-ray Diffraction Parameters for the (hkl) planes of Mint/Lemon Leaf TiO_2*

N°	Plan (hkl)	2θ (°)	d (Å)	Intensity (%)
1	(101)	25.32	3.51	100.0
2	(004)	37.86	2.37	17.7
3	(200)	48.06	1.89	31.6
4	(105)	53.97	1.70	20.4
5	(211)	55.09	1.67	17.2
6	(204)	62.76	1.48	12.0

The major peaks identified are consistent with those of TiO_2 anatase according to the JCPDS datasheet. The main peak located at 25.32° (2θ) corresponds to the (101) plane, typical of the anatase phase and dominant in nanostructured materials.

Phase confirmation and purity: No significant peaks attributable to the rutile (notably around 27.4° for the (110) plane) or brookite phases were observed. This confirms that the nanoparticles obtained are predominantly, if not exclusively, in the anatase form. The observed net crystallinity testifies to the structural quality of the material, despite green synthesis without organic solvents or extreme temperatures. The crystallite size, according to the Scherrer equation, is D = 325.4 Å = 32.5 nm.

3.1.4- BET Analysis:

BET analysis was used to determine the specific surface area of the synthesized (ZnO) and (TiO_2) nanoparticles. This method is based on the adsorption of nitrogen in the liquid state and allows for the evaluation of material porosity according to its adsorption capacity. Barrett-Joyner-Halenda (BJH) analysis, applied to the desorption branch of the isotherms, allowed for the estimation of the pore size distribution. These analyses revealed that the materials obtained predominantly exhibit a mesoporous structure.

a- BET Analysis – Nitrogen Adsorption / Desorption Isotherm for ZnOnp:

The nitrogen adsorption-desorption isotherms obtained for ZnO nanoparticles synthesized from clove/olive leaves **(A)** and mint/lemon leaves **(B)** highlight a behavior characteristic of mesoporous materials, with structural variations linked to the nature of the plant precursors, (**Fig. 9**).

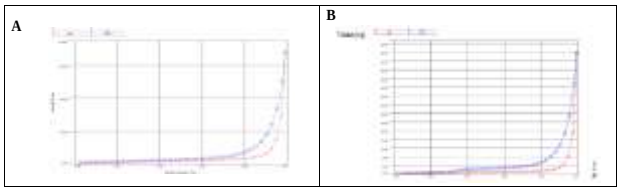

Figure 9: *Isothermal curve of ZnOnp adsorption/desorption from clove/olive leaves **(A)** and mint/lemon leaves **(B)***

The isotherm obtained for curve **A**, representing the adsorbed volume as a function of relative pressure (P/P_0), corresponds to a ***type II*** isotherm according to the IUPAC classification. This sigmoidal isotherm is characterized by a gradual adsorption at low pressure, followed by an abrupt increase in the adsorbed volume at high pressure. This behavior reflects the presence of multilayer adsorption and is typical of macroporous or low-porosity materials, where the initial interactions between the adsorbent and the adsorbate remain limited before the successive formation of several adsorption layers. The experimental conditions were as follows: Analysis gas: N_2, Temperature: 77.35 K (liquid nitrogen), Degassing time: 6 h at 180 °C, Sample mass: 1.3194 g.

A moderate increase in adsorbed volume was observed at low P/P_0 ratios, followed by marked growth from approximately $P/P_0 \approx 0.8$, indicating capillary adsorption within large pores, consistent with a poorly textured structure or one exhibiting macropores. These results confirm the macroporous nature of the material and its very low specific surface area (0.101 m^2/g), typical of ZnO biosynthesized from cloves and olive leaves.

The isotherm corresponding to curve **B**, which represents the adsorbed volume as a function of relative pressure (P/P_0), resembles a ***type III*** isotherm according to the IUPAC classification. This sigmoidal profile, lacking a marked plateau at high pressure, indicates a low initial affinity between the adsorbent and the adsorbate and is generally associated with mesoporous or low-porosity materials. The experimental conditions were as follows: Analysis gas: N_2, Temperature: 77.35 K (liquid nitrogen), Degassing time: 6 h at 180 °C, Sample mass: 1.3194 g.The isotherm shows relatively rapid adsorption at low pressures, followed by a pronounced increase in the adsorbed volume up to a near-plateau around $P/P_0 \approx 0.9$. This

behavior is characteristic of a capillary adsorption phenomenon within mesopores (2–50 nm), confirming the presence of an intermediate-sized porous structure.

***b- BJH Analysis – Pore Size Distribution* ZnOnp:** The BJH (Barrett–Joyner–Halenda) method used, based on the desorption curve, is standard for a reliable estimation of pore size.

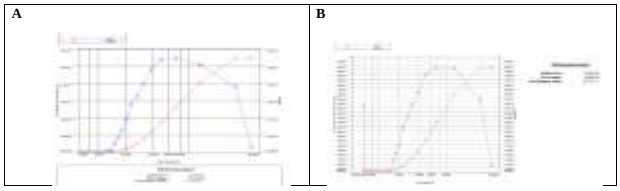

Figure 10:** BJH curve – ZnOnp pore size distribution of clove/olive leaves **(A)** and mint/lemon leaves **(B)

The results obtained according to curve **A** are summarized in the table below:

***Table 7:** BJH analysis results of ZnOnp from clove/olive leaf*

Parameter	Value	Interpretation
Specific surface area BET	26.156 m²/g	Moderate to relatively high for biosynthesized ZnO indicates a correct active surface, favorable to heterogenec processes (photocatalysis, adsorption).
Spore volume	0.219 cm³/g	Rather important — indicates an accessible porous netwo and good volumetric adsorption capacity.
Mean pore diameter (Dv(d))	157.110 Å (≈ 15.7 nm)	In the mesoporous range (≈ 2–50 nm), here towards the upp limit of the mesopores → presence of large pores interparticle spaces.

The BJH (dV/d log D) profile highlights a major peak centered between 150 and 300 Å (≈15–30 nm), indicative of large mesopores and interparticle voids. The peak width reflects a relatively wide pore distribution, a sign of moderate heterogeneity typical of materials synthesized via green processes, were biomolecules from plant extracts influence particle aggregation and organization **[35]**. ZnOnps prepared from mint and lemon leaves exhibit a mesoporous architecture (type IV isotherm), with an average pore diameter of 15.7 nm, a specific surface area of 26.2 m²/g, and a high pore volume (0.219 cm³/g). These characteristics indicate good accessibility of active

***Table 8:** BJH analysis results of ZnOnp from mint/lemon leaves*

Parameter	Value	Interpretation
Specific surface area BET	11.544 m²/g	Average – typical for biosynthesized ZnO. This indicates active surface area, useful for catalytic or antibacter applications.
Pore volume	0.090 cm³/g	Relatively modest, but consistent with mesoporous porosity.
Mean pore diameter (Dv(d))	29.737 Å (≈2.97 nm)	This diameter falls well within the mesoporous range (2– nm). This confirms that the nanoparticles have a mesoporc structure.

sites and make these nanoparticles promising for photocatalysis, adsorption, catalytic support, or the encapsulation of intermediate-sized molecules. The results obtained according to curve **B** are summarized in the table 8.The BJH curve shows a sharp peak around 30 Å (~3 nm), indicating that the majority of pores are of homogeneous size and around 3 nm, reflecting good pore homogeneity **[36]**. These nanoparticles exhibit a mesoporous structure with a ***type III*** isotherm, a uniform pore distribution (~3 nm), and a moderate specific surface area (11.5 m²/g). Potential applications include photocatalysis, pollutant adsorption, antimicrobial applications, and the transport and release of bioactive molecules.

c- BET Analysis – Nitrogen Adsorption/Desorption Isotherm Ti2Onp:

The adsorption-desorption isotherm of Ti_2O nanoparticles, providing information on porous texture, pore distribution and specific surface area, essential for characterizing their mesoporous structure.

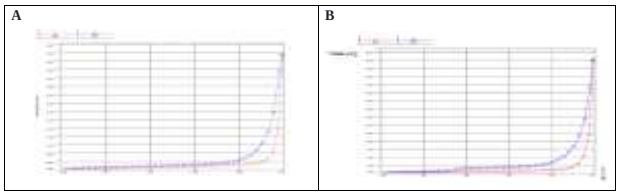

Figure 11:** Isothermal curve of adsorption/desorption of TiO2np from clove/olive leaves **(A)** and mint/lemon leaves **(B)

Isotherm type according to curve A: The nitrogen adsorption-desorption isotherm for curve A has a sigmoidal shape with hysteresis at high relative pressures ($P/P_0 \approx 0.8–1.0$), corresponding to a ***type IV*** isotherm according to the IUPAC classification, typical of mesoporous materials. This hysteresis reflects a progressive capillary filling of the mesopores **[35]**, followed by delayed desorption linked to nitrogen condensation and evaporation.

At low pressure ($P/P_0 < 0.2$), moderate adsorption reflects the formation of a nitrogen monolayer on the surface. In the intermediate zone ($0.4 < P/P_0 < 0.8$), the adsorbed volume gradually increases, indicating the gradual filling of the pores, while at high pressure ($P/P_0 > 0.8$), a sharp increase followed by a plateau reveals mesopore saturation. The observed hysteresis loop confirms the presence of open mesopores and illustrates the capillary condensation mechanism characteristic of these materials. Experimental conditions: N_2 gas, 77.35 K, degassing for 6 h at 180 °C, sample mass 1.3194 g.

Type of isotherm according to curve B: The nitrogen adsorption-desorption isotherm for curve B has a sigmoidal shape with hysteresis, characteristic of a type III isotherm according to the IUPAC classification, typical of mesoporous materials. The presence of hysteresis at high relative pressure ($P/P_0 \approx 0.8–0.9$) reflects a capillary adsorption mechanism

and progressive pore saturation **[35]**. At low pressure, significant initial adsorption is observed on the surface, while at high pressure ($P/P_0 \approx 0.9$), a plateau forms, indicating mesopore saturation and confirming the capillary adsorption phenomenon. Experimental conditions: Analysis gas: N_2, Temperature: 77.35 K (liquid nitrogen), Degassing time: 6 h at 180 °C, Sample mass: 1.3194 g, Instrument: Autosorb iQ Station 1.

d- BJH Analysis – Pore Size Distribution TiO2p : The method used was BJH (Barrett–Joyner–Halenda), based on the desorption curve, which is standard for a reliable estimation of pore size.

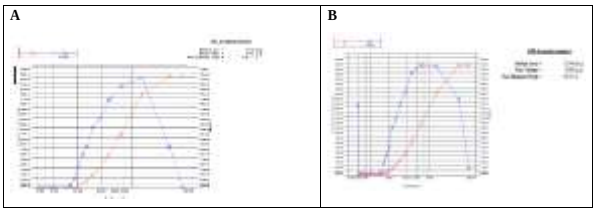

Figure 12: *BJH curve – TiO2np pore size distribution of clove/olive leaves* ***(A)*** *and mint/lemon leaves* ***(B)***

Results obtained according to curve **A** shown in the table below:

Table 9: *BJH Analysis Results of TiO2np from clove and olive leaves*

Parameter	Value	Interpretation
ecific surface area (BET)	0,101 m²/g	Very low — indicates virtually no available surface area (stro aggregation or sintering). Not well-suited for applicati requiring a large surface area (very active photocatalysis, h adsorption).
re volume	0,001 cm³/g	Extremely low — overall porosity almost non-existent; l volumetric adsorption capacity.
erage pore diameter	156,735 Å ≈ 15,7 nm	Relatively large mesopores (≈ 15–16 nm) — this value indica the presence of a few large pores or interparticle spaces rat than a fine, well-developed mesoporous network

The BJH (dV/d log D) curve highlights a broad peak centered around 156 Å (≈15.6 nm), indicating the presence of large mesopores, likely associated with interparticle spaces rather than finely developed internal porosity. The peak width reflects a wide pore distribution, revealing moderate heterogeneity, possibly resulting from partial agglomeration of the nanoparticles.

This morphology is consistent with the green synthesis based on olive leaves and cloves, where phenolic compounds (notably oleuropein and eugenol) act as reducing and stabilizing agents. The TiO_2 np thus synthesized exhibit:

• Mesoporous porosity (type IV isotherm) with an average pore diameter ≈15.6 nm;

• A very low specific surface area (0.101 m²/g) and a limited pore volume (0.001 cm³/g), indicating reduced accessibility of the active sites;

• An extensive pore distribution, likely due to agglomeration or densification occurring during calcination.

These characteristics give the nanoparticles properties suited to applications where diffusion is more important than active surface area, such as:

• High-temperature stable catalytic supports;

• Encapsulation materials or slow-release ion-exchange systems;

• Protective films and antimicrobial coatings.

The results obtained according to curve **B** shown in the table below:

Table 10: *BJH analysis results of TiO2np from mint/lemon leaves*

Parameter	Value	Interpretation
Specific surface area (BET)	11.544 m²/g	Moderate – typical of biosynthesized ZnO. Sufficient catalytic or antimicrobial applications.
Pore volume	0.090 cm³/g	Relatively low but typical for a mesoporous material.
Average pore diameter	29.737 Å (≈2.97 nm)	**In the mesoporous range** (2–50 nm), indicates homogeneous structure.

The BJH (dV/d log D) curve highlights a sharp peak around 30 Å (≈3 nm), indicating a narrow and homogeneous pore size distribution. This pore regularity suggests that the plant-based synthesis method (mint/lemon leaves) imparts good uniformity to the nanoparticle structure. TiO_2np synthesized via the green route from mint and lemon leaves exhibit:

• Mesoporous porosity (type III isotherm);

• A homogeneous pore distribution centered around ≈3 nm;

• A moderate specific surface area (11.5 m²/g), favoring several functional applications, such as:

o Photocatalysis (e.g., degradation of organic dyes);

o Adsorption of pollutants (heavy metals, organic molecules);

o Antimicrobial applications;

o Controlled encapsulation for nanomedicine.

3.1.5- Antimicrobial Activity: The evaluation of the antibacterial activity of titanium dioxide (TiO_2) and zinc oxide (ZnO) nanoparticles, synthesized from different plant extracts, revealed varying levels of efficacy depending on the bacterial strain tested. The results shown in Table **11** demonstrated that:

Table 11: *Results of the antimicrobial study*

Microbial strains	Result	Diameter (cm)
Staphylococcus aureus	Moderate to high activity	4 = 0.8 ; 5 = 1.4 ; 6 = 0.9 ; 7 = 1.0
Escherichia coli	Low to moderate activity	4 = 0.9 ; 5 = 1.0 ; 6 = 0.8 ; 7 = 1.0
Pseudomonas aeruginosa	No activity	/

• *Against Staphylococcus aureus* (Gram-positive), the TiO_2–olive/clove sample (No. 5) exhibited the largest inhibition zone (1.4 cm), indicating strong

antibacterial activity. The other formulations showed moderate activity, with diameters ranging from 0.8 to 1 cm.

• *Against Escherichia coli* (Gram-negative), all the tested nanoparticles showed lower activity than against S. aureus. Sample No. 5 (TiO_2–olive/clove) remained the most effective (1 cm), while the other samples showed inhibition zones between 0.8 and 0.9 cm.

• *Against Pseudomonas aeruginosa*, no inhibitory effect was observed for any of the tested samples, indicating high resistance of this strain to the studied nanoparticles **[36-37]**. Overall, the results demonstrate that TiO_2 nanoparticles, particularly those derived from the olive leaf/clove combination, exhibit the best antibacterial efficacy among the tested formulations. ZnO nanoparticles showed adequate activity, but overall, it was lower than that of TiO_2. The lack of activity against Pseudomonas aeruginosa suggests the need to optimize formulations or concentrations to target highly resistant bacteria.

3.2- Discussion:

3.2.1- UV-Vis: UV-Vis analyses confirm the formation of ZnO and TiO_2 nanoparticles, with typical absorption peaks around 380–400 nm and 330–370 nm, respectively. ZnO and TiO_2 synthesized from clove and olive leaves show a slight redshift, indicating greater crystallinity and a larger particle size, while those from mint and lemon show a blueshift, indicating finer particles. These differences result from the nature of the secondary metabolites in the plant extracts, which act as reducing and stabilizing agents, influencing the size, morphology, and stability of the nanoparticles**.**

3.2.2- IR: FTIR analysis confirmed the formation of zinc oxide (ZnO) and titanium dioxide (TiO_2) nanoparticles synthesized via a green process from plant extracts. The spectra revealed the disappearance of the characteristic zinc nitrate (NO_3^-) bands and the appearance of new bands in the 480–590 cm^{-1} (Zn–O) and 680–780 cm^{-1} (Ti–O) regions, confirming the formation of the metal oxides. The bands observed around 3400 cm^{-1} and 1600 cm^{-1} indicate the presence of OH and C=O/C=C groups, linked to phenolic compounds, flavonoids, and other biomolecules in the plant extracts. These biomolecules play an essential role as reducing and stabilizing agents during the synthesis. Thus, the simultaneous presence of organic and inorganic bands confirms that the green synthesis allowed not only the formation of ZnO and TiO_2, but also their stabilization by secondary metabolites from the plant extracts used.

3.2.3- XRD: X-ray diffraction (XRD) analysis confirmed the formation and crystal structure of the zinc oxide (ZnO) and titanium dioxide (TiO_2) nanoparticles synthesized via the green route. The recorded diffractograms show intense and well-defined peaks, indicating excellent crystallinity of the materials obtained. For the ZnO nanoparticles, the characteristic peaks observed at $2\theta \approx 31.8°$, 34.4°, 36.2°, 47.5°, 56.6°, and 62.8° correspond respectively to the (100), (002), (101), (102), (110), and (103) planes, confirming the hexagonal wurtzite phase of ZnO, in accordance with JCPDS 98-016-5002. The absence of spurious peaks indicates the purity of the phase and the efficiency of the biological reduction. The good crystallinity and nanometric size (≈33.5 Å) suggest regular crystallite growth, promoted by the bioactive compounds (phenols, flavonoids, tannins) of the extracts used.

For TiO_2nps, the major peaks located at $2\theta \approx 25.3°$, 37.8°, 48.0°, 53.9°, 55.0°, and 62.7° correspond to the (101), (004), (200), (105), (211), and (204) planes, characteristic of the anatase phase according to JCPDS 98-017-2914 and 98-008-2084. The absence of peaks associated with the rutile or brookite phases confirms the purity of the anatase phase, which is the most reactive and the most sought-after for photocatalytic and antimicrobial applications. The average crystallite size, estimated at approximately 32.5 nm, reflects efficient nanostructuring induced by green synthesis.Overall, the comparison between the extracts shows that the clove/olive leaf mixtures lead to slightly higher crystallinity, while the mint/lemon leaf extracts produce slightly finer nanoparticles. These differences reflect the direct influence of the chemical composition of the plant extracts on the nucleation and growth of crystallites. These results demonstrate that biogenic synthesis is an environmentally friendly, simple, and efficient approach for obtaining high-purity crystalline ZnO and TiO_2 nanoparticles, comparable to those produced by conventional chemical processes.

3.2.4- BET: BET and BJH analyses highlighted the significant influence of the type of plant extract on the textural properties of the resulting nanoparticles. The results show that the ZnO and TiO_2 biosynthesized from mint and lemon leaf extracts exhibit higher specific surface areas and greater porosity than those produced from clove and olive leaves. This difference can be attributed to the chemical nature of the biomolecules present in the plant extracts: the phenolic compounds, flavonoids, and organic acids of mint and lemon act not only as reducing agents but also as stabilizing agents, limiting nanoparticle aggregation and promoting the formation of homogeneous mesopores.In contrast, the heavy, oily compounds in clove and olive tend to

cause agglomeration and network densification, thus reducing the specific surface area and pore volume. The mesoporous nature of the materials, confirmed by BJH curves (with average pore diameters between 3 and 16 nm), is favorable for applications requiring high accessibility of active sites, such as photocatalysis, pollutant adsorption, and antimicrobial applications. The high pore volume values (up to 0.219 cm^3/g) for ZnO (mint/lemon) confirm an open structure that allows for good diffusion of reactive molecules, which enhances their potential in catalytic and environmental processes.Furthermore, the comparison between ZnO and TiO_2 reveals that ZnO nanoparticles generally possess larger specific surface areas and pore volumes, which explains their greater expected efficiency in photo-induced reactions. TiO_2, although mesoporous, exhibits smaller surface areas, indicating less dispersion or more pronounced agglomeration after calcination. In summary, the combination of BET and BJH analyses demonstrates that the green biosynthesis method directly influences the microstructure and texturing of metal oxides, and that judicious selection of the plant extract allows for the optimization of the physicochemical properties of the final material.

3.2.5- Antimicrobial Activity: The results obtained during the evaluation of the antibacterial activity of zinc oxide nanoparticles (ZnO NPs) and titanium dioxide nanoparticles (TiO_2 NPs), synthesized from medicinal plant extracts, revealed significant differences in efficacy depending on the type of nanoparticle, the nature of the plant extract used, and the bacterial strain tested. TiO_2 nanoparticles combined with olive leaf and clove extracts (sample no. 5) showed the strongest antibacterial activity, particularly against Staphylococcus aureus (zone of inhibition of 1.4 cm). This result can be attributed to the synergy between TiO_2 and the bioactive compounds present in the plant extracts, such as phenols, flavonoids, terpenoids, and eugenol, known for their antimicrobial properties. These secondary metabolites can facilitate the attachment of nanoparticles to the bacterial cell wall and increase membrane permeability, leading to leakage of cell contents and bacterial death.The moderate activity observed against Escherichia coli can be explained by the more complex structure of the outer membrane of Gram-negative bacteria, which acts as an additional barrier preventing the efficient penetration of nanoparticles. Despite this, TiO_2 doped with extracts rich in phenolic compounds maintained appreciable activity, suggesting a significant interaction between the bioactive agents and the nanoparticles. In contrast, the lack of inhibitory effect observed against Pseudomonas aeruginosa confirms the high natural resistance of this species, often attributed to biofilm formation, the low permeability of its outer membrane, and the presence of active efflux systems. These mechanisms considerably reduce the effectiveness of metallic nanoparticles, even at high concentrations. ZnO nanoparticles, although exhibiting measurable antibacterial activity, showed lower efficacy than TiO_2. This behavior could be linked to differences in particle size, ionic solubility, or the ability to generate reactive oxygen species (ROS), which play a key role in antimicrobial action. In general, these results are consistent with several previous studies that have demonstrated that metal oxide nanoparticles obtained via green processes exhibit antibacterial activity dependent on the nature of the metal, the bacterial strain, and the type of plant extract used for their synthesis.

4- Conclusions

The analytical results confirm the successful formation of ZnO and TiO_2 nanoparticles obtained via a green process from plant extracts. UV-Visible spectra reveal characteristic absorption bands around 380–400 nm for ZnO and 330–370 nm for TiO_2, confirming the formation of metal oxides. Variations in the observed maxima between extracts show that the richness in phenolic metabolites strongly influences particle size, crystallinity, and stability, with clove and olive extracts promoting increased crystallinity, while mint and lemon extracts lead to finer and more stable particles. FTIR analysis also confirmed the formation of Zn–O and Ti–O metal bonds across bands located between 480–590 cm^{-1} and 680–780 cm^{-1}, respectively. The presence of signals associated with hydroxyl, carbonyl, and aromatic groups demonstrates the involvement of bioactive compounds in the reduction and stabilization of the nanoparticles, thus reinforcing the potential of biogenic synthesis as a green and sustainable approach. XRD analyses revealed characteristic diffractograms of ZnO in its hexagonal wurtzite form and of TiO_2 in its anatase phase, with no impurities detected. The estimated crystallite sizes, between 30 and 35 nm, confirm the nanometric nature and good crystallinity of the materials obtained, highlighting the effective role of plant extracts as reducing and stabilizing agents. The BET/BJH textural analysis showed that the nanoparticles predominantly exhibit a mesoporous structure. Extracts of mint and lemon leaves generated materials with a higher specific surface area, a large pore volume, and a regular pore size distribution, unlike those derived from clove and olive, which are more prone to agglomeration. These characteristics give the former a significant advantage for photocatalytic, adsorptive, and

antimicrobial applications. Finally, antimicrobial evaluations highlighted the greater activity of TiO_2 nanoparticles, particularly those synthesized from olive and clove leaves, suggesting a synergy between the material and the phytochemical compounds. However, the notable resistance of Pseudomonas aeruginosa indicates the need to explore complementary strategies such as metal doping or combination with antibiotics.Overall, these results demonstrate that biogenic synthesis is an ecological, economical and efficient approach for the development of stable, pure and functional nanoparticles, with strong potential for environmental and biomedical applications.

Author Statements:

- **Ethical approval:** The conducted research is not related to either human or animal use.
- **Conflict of interest:** The authors declare that they have no known competing financial interests or personal relationships that could have appeared to influence the work reported in this paper
- **Acknowledgement:** The authors declare that they have nobody or no-company to acknowledge.
- **Author contributions:** The authors declare that they have equal right on this paper.
- **Funding information:** The authors declare that there is no funding to be acknowledged.
- **Data availability statement:** The data that support the findings of this study are available on request from the corresponding author. The data are not publicly available due to privacy or ethical restrictions.

References

[1] Petersen, P. E., & Ogawa, H. (2012). The global burden of periodontal disease: towards integration with chronic disease prevention and control. Periodontology 2000, 60(1), 15–39. DOI : 10.1111/j.16000757.2011.00425.x

[2] Raut, J. S., & Karuppayil, S. M. A. (2014). status review on the medicinal properties of essential oils. Industrial Crops and Products, 62, 250–264. https://doi.org/10.1016/j.indcrop.2014.05.055

[3] Kumar R, Mirza MA, Naseef PP, Kuruniyan MS, Zakir F, Aggarwal G. (2022) : Exploring the potential of natural product-based nanomedicine for maintaining oral health. Molecules., 27(5) :1725.
https://doi.org/10.3390/molecules 27051725

[4] Morowvat MH, Kazemi K, Jaberi MA, Amini A. (2023). Gholami A: Biosynthesis and antimicrobial evaluation of zinc oxide nanoparticles using Chlorella vulgaris biomass against multidrug-resistant pathogens. Materials (Basel). 16 (2):842.
https://doi.org/10.3390/ma16020842

[5] Zahraa A. Abdul Muhsin, Ghaith H. Jihad, et Liath. A. Yaaqoob.(2025): Green Synthesis of ZnO–TiO_2 Nanoparticles Using Allium ampeloprasum (Kurrat) Extract and Their Antibacterial Activity. ASEAN J. Sciences. Technologie. Rapport., 28(4), e256572.
https://doi.org/10.55164/ajstr.v28i4.256572

[6] Raghupathi, K.R., Koodali, R.T., & Manna, A.C. (2011). Size-dependent bacterial growth inhibition and mechanism of antibacterial activity of zinc oxide nanoparticles. Langmuir, 27(7), 4020–4028.
DOI: 10.1021/la104825u

[7] Yao Tu, Li Zhou, Yi Zheng Jin, Chao Gao, Zhi Zhen Ye, Ye Feng Yang and al. (2010): *Transparent and flexible thin films of ZnO-polystyrene nanocomposite for UV-shielding applications*, Journal of Materials Chemistry, N°8.

[8] Suddhasattya Dey, Dibya lochan Mohanty., and al. (2025). A critical review on zinc oxide nanoparticles: Synthesis, properties and biomedical applications. Intelligent Pharmacy, Volume 3, Issue 1, Pages 53-70.
https://doi.org/10.1016/j.ipha.2024.08.004

[9] Getaneh Diress Gesesse. (2021). "Photocatalytic and photoelectrochemical study of mixed semiconductor/carbon nanoporous materials catalysts: Application to the degradation of environmental pollutions" Thèse de doctorat.

[10] Anker, J.N., Hall, W.P., Lyandres, O., Shah, N.C., Zhao, J., & Van Duyne, R.P. (2008). Biosensing with plasmonic nanosensors. Nature Materials, 7(6), 442–453.
DOI: 10.1038/nmat2162

[11] Sun, Y., & Xia, Y. (2002). Shape-controlled synthesis of gold and silver nanoparticles. Science, 298(5601), 2176–2179.
DOI : 10.1126/science.1077229

[12] Marion Stalet. (2024). Antimicrobial protection: combining functionalization and nano-structuring to explore cell-surface interactions, HAL.
https://theses.hal.science/tel-04651199v1

[13] Prashar, A., Locke, I. C., & Evans, C. S. (2006). *Cytotoxicity of clove (Syzygium aromaticum) oil and its major components to human skin cells. Cell Proliferation*, 39(4), 241–248.
DOI: 10.1111/j.1365-2184.2006.00384x

[14] Bakkali, F., Averbeck, S., Averbeck, D., & Idaomar, M. (2008). *Biological effects of essential oils – A review. Food and Chemical Toxicology*, 46(2), 446–475.
https://doi.org/10.1016/j.fct.2007.09.106

[15] Omar, S. H. (2010). *Oleuropein in olive and its pharmacological effects. Scientia Pharmaceutica*, 78(2), 133–154.
doi: 10.3797/scipharm.0912-18

[16] Visioli, F., Poli, A., & Galli, C. (2002). *Antioxidant and other biological activities of phenols from olives and olive oil. Medicinal Research Reviews*, 22(1), 65–75.
DOI: 10.1002/med.1028

[17] González-Molina, E., Domínguez-Perles, R., Moreno, D. A., & García-Viguera, C. (2010). Natural bioactive compounds of citrus limon for

food and health. Journal of Pharmaceutical and Biomedical Analysis, 51(2), 327–345.
DOI : 10.1016/j.jpba.2009.07.027

[18] Giacomo Luigi Petretto, Giuseppe Vacca , et al, (2023). Waste Citrus limon Leaves as Source of Essential Oil Rich in Limonene and Citral: Chemical Characterization, Antimicrobial and Antioxidant Properties, and Effects on Cancer Cell Viability, PubMed; 12(6):1238.
https://doi.org/10.3390/antiox12061238

[19] McKay, D. L., & Blumberg, J. B. (2006). *A review of the bioactivity and potential health benefits of peppermint tea (Mentha piperita L.).* Phytotherapy Research, 20(8), 619–633.
DOI: 10.1002/ptr.1936

[20] Singh, R., Shushni, M. A. M., & Belkheir, A. (2015). *Antibacterial and antioxidant activities of Mentha piperita L.* Arabian Journal of Chemistry, 8(3), 322–328.
https://doi.org/10.1016/j.arabjc.2011.01.019

[21] Aldrin J, Rajeshkumar S, Ezhilarasan D, Lakshmi T. (2022): Comparative antimicrobial effect of mouthwash prepared using herbal formulations of Stevia and Ficus benghalensis mediated silver nanoparticles. Int J Early Child Spec Educ., Vol 14, Issue 03.
DOI:10.9756/INT-JECSE/V1413.408.

[22] Rajeshkumar S, Parameswari RP and al. (2023). Green synthesis, characterization and bioactivity of Mangifera indica seed-wrapped zinc oxide nanoparticles. Molecules.,21;28(6):2818. DOI: 10.3390/molecules28062818

[23] Ramesh, M., Anbuvannan, M., & Viruthagiri, G. (2015). *Green synthesis of ZnO nanoparticles using Solanum nigrum leaf extract and their antibacterial activity. Spectrochimica Acta Part A: Molecular and Biomolecular Spectroscopy, 136*, 864–870,.
https://doi.org/10.1016/j.saa.2014.09.105

[24] M. Sundrarajan, S. Ambika, K. Bharathi. (2015). Plant-extract mediated synthesis of ZnO nanoparticles using Pongamia pinnata and their activity against pathogenic bacteria. Advanced Powder Technology. V 26, numéro 5 , p 1294-1299.
https://doi.org/10.1016/j.apt.2015.07.001

[25] Subhapriya, S., & Gomathipriya, P. (2018). Green synthesis of titanium dioxide (TiO_2) nanoparticles by Trigonella foenum-graecum extract and its antimicrobial properties, Microbial Pathogenesis, V 116, P 215-220.
DOI: 10.1016/j.micpath.2018.01.027

[26] Jagpreet Singh, Tanushree Dutta, Ki-Hyun Kim, Mohit Rawat, Pallabi Samddar & Pawan Kumar. (2018). 'Green' synthesis of metals and their oxide nanoparticles: applications for environmental remediation, Journal of Nanobiotechnology, 16, Article number: 84.
https://doi.org/10.1186/s12951-018-0408-4

[27] Tiwari, A.K., Jha, S., Tripathi, S.K., Shukla, R., Awasthi, R.R., Bhardwaj, A.K., Singh, A.K., Dikshit, A. (2024). "Spectroscopic investigations of green synthesized zinc oxide nanoparticles (ZnO NPs): antioxidant and antibacterial activity." *Discover Applied Sciences*, 6, Article 399.
https://doi.org/10.1007/s42452-024-06049-z

[28] Sasani Ghamsari M, Alamdari S, Han W, Park HH. (2017). Impact of nanostructured thin ZnO film in ultraviolet protection. Int J Nanomed. V 2017: 12, p 207-216
DOI: https://doi.org/10.2147/IJN.S118637

[29] Kangqiang Huang, Li Chen, Jieguan Deng, and Jianwen Xiong. (2012). Enhanced Visible-Light Photocatalytic Performance of Nanosized Anatase TiO2 Doped with CdS Quantum Dots for Cancer-Cell Treatment, Journal of Nanomaterials, p 12.
DOI: 10.1155/2012/720491

[30] Nusrat Jahan Tamanna and al. (2024). Easy and green synthesis of nano-ZnO and nano-TiO_2 for efficient photocatalytic degradation of organic pollutants, Heliyon 10, e37469.
DOI:10.1016/j.heliyon.2024.e37469

[31] Leirika Ngangom , Kunal Sharma and al. (2025). Green synthesis, characterization and antibacterial potential of zinc oxide nanoparticles with naringenin, BMC Pharmacol Toxicol. 26:170.
doi: 10.1186/s40360-025-00974-4

[32] Mohammad Zaki Ahmad, Ali S. Alasiri. (2022). Green Synthesis of Titanium Dioxide Nanoparticles Using *Ocimum sanctum* Leaf Extract: In Vitro Characterization and Its Healing Efficacy in Diabetic Wounds, *Molecules*, *27*(22), 7712.
https://doi.org/10.3390/molecules27227712

[33] Shahla Hashemi, Zahra Asrar, and al. (2016). Green synthesis of ZnO nanoparticles by Olive (*Olea europaea*), IET Nanobiotechnol, 1;10(6):400–404,
doi: 10.1049/iet-nbt.2015.0117

[34] Mohammad Zaki Ahmad, Ali S. Alasiri, and al. (2022). Green Synthesis of Titanium Dioxide Nanoparticles Using Ocimum sanctum Leaf Extract: In Vitro Characterization and Its Healing Efficacy in Diabetic Wounds, Molecules, 27, 7712.
https://doi.org/10.3390/molecules27227712

[35] Rab Nawaz, Habib Ullah, and al. (2023). Green Synthesis of ZnO and Black TiO_2 Materials and Their Application in Photodegradation of Organic Pollutants, *ACS Omega*, Vol 8/Issue 39, 36076-36087.
https://doi.org/10.1021/acsomega.3c04229

[36] Sushma Khatri, Dharma Prasad Khanal. (2024). Synthèse verte de nanoparticules d'oxyde de zinc utilisant extrait de feuilles Mangifera indica L. et évaluationde son activité antibactérie, Journal asiatique de pharmacognosy, 8(4):1-22.

[37] Nasir Shakeel , Ireneusz Piwoński, Parvaz Iqbal, Aneta Kisielewska. (2025). Green Synthesis of Titanium Dioxide Nanoparticles: Physicochemical Characterization and Applications: A Review, *International Journal of Molecular Sciences*, 6;26(12):5454.doi: 10.3390/ijms26125454